The International Journal of Advanced Manufacturing Technology (2018) 98:1339–1353
https://doi.org/10.1007/s00170-018-2292-3

ORIGINAL ARTICLE

Research and development of the asymmetric grayscale roll-to-plate processing technology

Yung-Jin Weng [1]

Received: 16 March 2018 / Accepted: 4 June 2018 / Published online: 19 June 2018

Abstract
This study aims to propose a novel roll-to-plate (R2P, was proposed a roller press mechanism that flat-type flexible mold soft cylindrical stamps is used to provide the imprinting force onto a rigid surface) technology with a flexible micro/nanoscale structures and takes it as the microstructure for producing an innovative continuous asymmetric grayscale microstructures (linear gradient microstructure arrays replication). This study first calculated and simulated the mechanical effect that affects the microstructures geometrical shape and R2P after the asymmetric grayscale inclined R2P. At the same time, this study developed and set up an innovative asymmetric grayscale (R2P) imprinting system with the micro/nanoscale structure component. During the development process, the existing gas-assisted light-curing technology was adopted, and the mold core of the flexible micro/nanoscale structures with gas pressurization. By integrating UV curing technology, this study adopted the continuous grayscale inclination method to create the R2P microstructure on the flexible model of the polymer, in order to obtain a continuous and large-area asymmetric grayscale microstructure. The test results suggested that the microstructure layer had thick mold, the elastic modulus provided higher and wider pressure distribution to the resist, and the symmetrical force was uniform. Moreover, there was significant grayscale pressure distribution under asymmetric force. Under the condition that the flexible microstructure mold core is too soft, it shows that the opportunity for the slight inclined-rotation effect of the microstructure occurs between the R2P. The proposed technology is expected to optimize the existing backlight module space and improve the light diffusion uniformity. In addition to providing a convenient and fast-forming mechanism, the proposed technology can effectively reduce the thickness of the flexible backlight module and produce a thin flexible display panel.

Keywords Microstructure · Asymmetric · Gray-scale · Flexible mold · Roll-to-plate (R2P)

1 Introduction

The realization of Moore's law allows micro/nanoscale manufacturing technology to be continuously developed and innovated, thereby accommodating more micro/nanoscale components or microstructures within the unit area. At the same time, smooth operation and industrialization under the micro/nanoscale scale are key issues to be considered. Roll-to-plate (R2P) forming technology and R2P forming technology are critical in the mass production that uses microsystem technology, which are featured in the mass production of electronic microcomponents [1], medical testing microcomponents [2, 3], display microstructure backlight modules [4–7], etc. This technology has capabilities of fast operation mass production and the development of related time efficiency. Micro/nanoscale components can provide energy to directly or indirectly enhance current technological development. For example, in the manufacturing of the micro-fluidic channels of nano-biomedical components, it can assist the screening of cancer cells. By comparing the movement distance of normal cells and cancer cells according to the passage time of the cells through the holes and the same pressure in the fixed time [8, 9], the presence of cancer cells can be determined. In photoelectric transmission, micro/nanoscale components can be used as a medium for conducting light wave energy, such as the realization of the optical waveguide microstructure component [10–15]. By taking the polymer material as a medium to transmit light wave energy, the wire size can be greatly reduced to improve the energy transfer effect. The micro/nanoscale structure components on the optical display are also

✉ Yung-Jin Weng
yjweng@mail.ncyu.edu.tw

[1] Department of Mechanical and Energy Engineering, National Chiayi University, No. 300, Syuefu Road, Chiayi City 600, Taiwan

useful for the light diffusion effect (diffusion plate microstructures), the spectral effect (grating arrays), and light condensation (microlens arrays), all of which play important roles in the display manufacturing [16, 17]. R2P or R2R is a technique for the mass production of MEMS, as well as for simplifying and optimizing the processing speed of MEMS components. Therefore, this study aimed to develop an Asymmetric grayscale R2P processing technology, specifically an asymmetric grayscale R2P embossing replication system machine. With the simulation and physical structure of a microstructure mold core, continuous grayscale R2P can be conducted at different angles with the adjustable asymmetric microstructure. The results were compared with the setting in order to verify the microstructure shape obtained under the setting of asymmetric embossing and confirm the accuracy of the proposed technology.

2 Geometric pattern and prediction of the asymmetric R2P microstructure

2.1 Asymmetric R2P simulation material parameters and roller angle positioning method

The simulation was conducted using engineering simulation Matlab software. The characteristic scale of the roller simulation was the same as the R2P system developed by this study, as shown in Fig. 1. The material parameters used in the simulation of this study were the material mechanical properties measured by a nanoindenter [18, 19] and the microtensile testing machine produced by Instron, as shown in Table 1. In addition, roller angle positioning used the geometric approach to conduct a pre-embossing positioning assessment. As the roller is curved, the positioning design used the microstructure on the roller as the relative embossing angle of the replication material. The shape of the microstructure, as produced by the R2P at the same time, was determined as the asymmetric angle, which is the initial depression angle.

2.2 Asymmetric rolling principle transformation

The system layout is illustrated as shown in Fig. 2a, the coordinate system $x-y-z$ is a fixed reference coordinate frame, and its origin is set to lay on the center and pivot of plane E_{model}. E_{model} is the plane where microstructure array models are attached on it, and $E_{pattern}$ is the plane where the nanoimprint patterns are produced on it. h is the distance between the planes E_{model} and $E_{pattern}$. Suppose a point p laid on the surface of the model which attached on plane E_{model}. Point p can be represented by vector rp in the coordinate system $x-y-z$. The coordinate system $x-y-z$ is a fixed coordinate system, we treat it as a fixed reference and mechanical coordinate system in our deduction process. When plane E_{model} has performed oblique operation, the position of point p has changed in views of fixed reference coordinate system $x-y-z$. The new

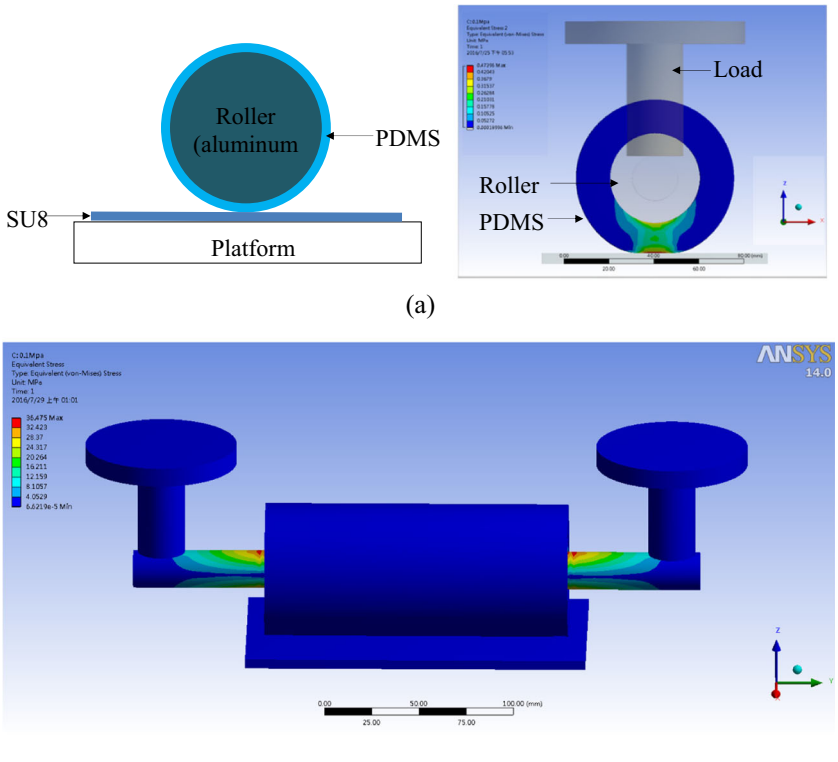

Fig. 1 Roller simulation. **a** End view. **b**) Side view

Table 1 Material mechanical properties measured by nanoindenter and tensile testing (proportion (A/B))

Types	Elastic modulus (MPa)	Poisson's ratio
Nanoindentation (10:1)	3.45	0.51
Tensile test (10:1)	1.72	0.495
Tensile test (5:1)	2.20	0.52

position of point p is denoted as $p_{\varnothing\theta}$ and represent by vector $\boldsymbol{r}_{\varnothing\theta}$. The connection between vector $\boldsymbol{r}_{\varnothing\theta}$ and vector $\boldsymbol{r}_p$ can be constructed by the transformation matrix $U_{\varnothing\theta}$. Vector $\boldsymbol{r}_{p\varnothing\theta}$ can then be obtained by the following equation:

$$\boldsymbol{r}_{p\varnothing\theta} = U_{\varnothing\theta p}\boldsymbol{r} \tag{1}$$

To construct the transformation matrix $U_{\varnothing\theta}$, we perform the following operation. At first, we make a real and substantial operation. We try to get the new position of point p, denoted as $P_{r\to\varnothing\theta\to r'/}$, which represented by vector $\boldsymbol{r}_{r\to\varnothing\theta\to r'/}$ in terms of coordinate system $x''-y''-z''$ after the oblique operation was performed. The oblique operation is a real and substantial operation; it transforms the point p into a new position denoted by point $P_{r\to\varnothing\theta\to r'/}$ and meanwhile transforms the vector $\boldsymbol{r}_p$ into a new vector denoted by $\boldsymbol{r}_{r\to\varnothing\theta\to r'/}$. We decompose the oblique operation into two subsequent operations: the first is ∅rotation operation, and the second is θ rotation operation. For ∅rotation operation, we establish a new coordinate system $x'-y'-z'$ which can be obtained by taking z axis of coordinate system $x-y-z$ as rotation axis and rotate counterclockwise coordinate system $x-y-z$ by an angle ∅. So for any of the components of vector $\boldsymbol{r}_p$, says x, the x component of vector $\boldsymbol{r}_p$, can be decomposed into x' and y' components in coordinate system $x'-y'-z'$. That is $\mathbf{x}=x\hat{x} = x\cos\varnothing\widehat{x'} - x\sin\varnothing\widehat{y'}$ where x is the magnitude of x component and $\hat{x}$ is the unit vector of x axis in coordinate system $x-y-z$, x' and y' are the unit vectors of x' and y' axes in coordinate system $x'-y'-z'$, respectively, as shown in Fig. 2b. For θ rotation operation, a new coordinate system $x''-y''-z''$ is established. It is obtained by taking the y' axis of coordinate system $x'-y'-z'$ as the rotation axis and rotate counterclockwise coordinate system $x'-y'-z'$ by an angle θ. At this moment, the component $x\cos\varnothing\widehat{x'}$ laid originally in coordinate system $x'-y'-z'$ is shifted to $x\cos\varnothing\widehat{x'}$ where $\widehat{x'/}$ is the unit vector of x'' axis in coordinate system $x''-y''-z''$. And the component $-x\sin\varnothing\widehat{y'}$ does not change during this θ rotation operation because that $\widehat{y'}$ and $\widehat{y'/}$ are coincident in both coordinate systems $x'-y'-z'$ and $x''-y''-z''$ as shown in Fig. 2c. That is, we have $-x\sin\varnothing\widehat{y'} = -x\sin\varnothing\widehat{y'/}$. So far, we have seen that the original component xbx in coordinate system $x-y-z$ is transformed into $x\cos\varnothing\widehat{x'/} - x\sin\varnothing\widehat{y'/}$ in the coordinate system $x''-y''-z''$. That is, we get the coordinate of the vector $x\widehat{x'/}$ when the oblique operation has performed, the coordinate of the new position of point p, that is point $P_{r\to\varnothing\theta\to r'/}$, is represent by the vector $x\cos\varnothing\widehat{x'/} - x\sin\varnothing\widehat{y'/}$ in coordinate system $x''-y''-z''$.

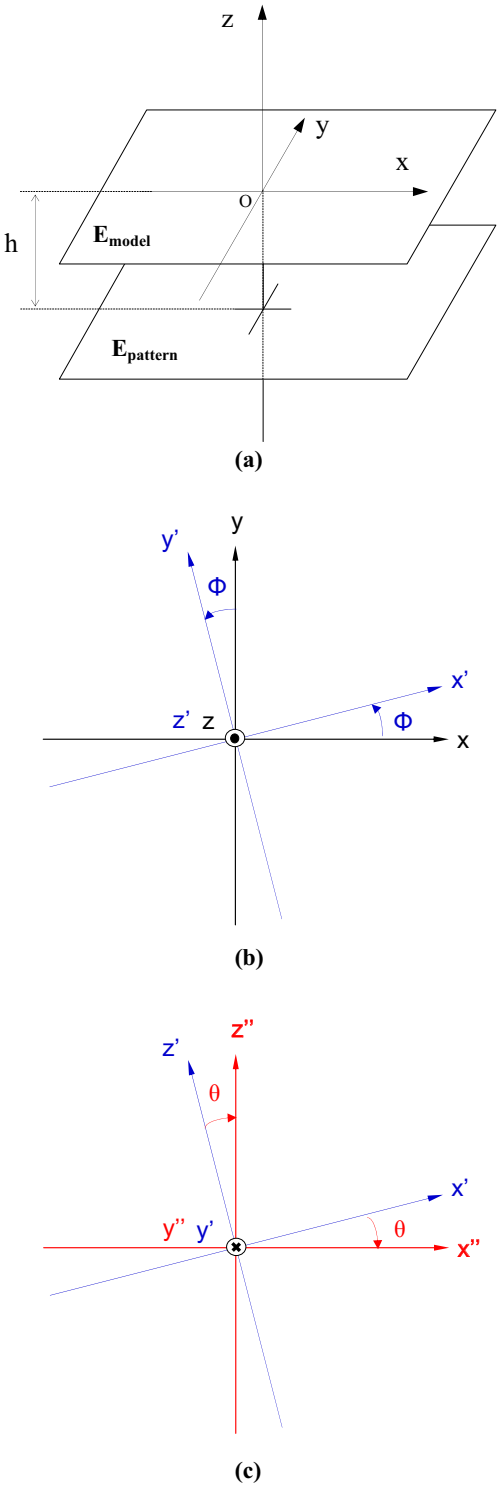

Fig. 2 **a** System layout. **b** First step, ∅ rotation. **c** First step, θ rotation

Following the similar deduction procedures as done for the x components of vector $\boldsymbol{r}_p$ shown above, we can get the coordinates of y and z components of vector $\boldsymbol{r}_p$ to be represented in terms of coordinate system $\mathrm{x}''-\mathrm{y}''-\mathrm{z}''$ when the oblique operation has performed. So, we find that y component can be transformed into $y\sin\varnothing\widehat{x'} + y\cos\varnothing\widehat{y'}$ and z component can be transformed into $z\widehat{z'}$ in the coordinate system $\mathrm{x}''-\mathrm{y}''-\mathrm{z}''$ after the oblique operation performance. Summarizing the above deductions, we have

$$\left\{\begin{array}{c} x\hat{x} = x\cos\varnothing\widehat{x'} - x\sin\varnothing\left(-\widehat{y'}\right) = x\cos\varnothing\widehat{x''} + (-x\sin\varnothing)\widehat{y''} \\ y\hat{y} = y\sin\varnothing\widehat{x'} + y\cos\varnothing\widehat{y'} = y\sin\varnothing\widehat{x''} + y\cos\varnothing\widehat{y''} \\ z\hat{z} = z\widehat{z'} = z\widehat{z''} \end{array}\right\} \quad (2)$$

We can write down the transformation matrix between coordinate systems $\mathrm{x}''-\mathrm{y}''-\mathrm{z}''$ and $x-y-z$; the transformation matrix describes that vector $\boldsymbol{r}_p$ in the coordinate system $x-y-z$ becomes vector $\boldsymbol{r}_{p_{r\to\varnothing\theta\to r''}}$ in the coordinate system $\mathrm{x}''-\mathrm{y}''-\mathrm{z}''$ after the oblique operation performance.

$$\begin{pmatrix} x'' \\ y'' \\ z'' \end{pmatrix}_{r''} = \begin{pmatrix} \cos\varnothing & \sin\varnothing & 0 \\ -\sin\varnothing & \cos\varnothing & 0 \\ 0 & 0 & 1 \end{pmatrix} \begin{pmatrix} x \\ y \\ z \end{pmatrix}_{r} \quad (3)$$

The transformation operation can be represented in a contracted form

$$\boldsymbol{r}_{p_{r\to\varnothing\theta\to r''}} = \boldsymbol{U}_{p_{r\to\varnothing\theta\to r''}}\boldsymbol{r}_p \quad (4)$$

with transformation matrix

$$U_{r\to\varnothing\theta\to r''} = \begin{pmatrix} \cos\varnothing & \sin\varnothing & 0 \\ -\sin\varnothing & \cos\varnothing & 0 \\ 0 & 0 & 1 \end{pmatrix} \quad (5)$$

Next, we have to transform the vector $\boldsymbol{r}_{p_{r\to\varnothing\theta\to r''}}$ represented in terms of coordinate system $\mathrm{x}''-\mathrm{y}''-\mathrm{z}''$ back to $\boldsymbol{r}_{p\varnothing\theta}$ represented in terms of coordinate system $x-y-z$. The operation is not a real and substantial operation as the first operation shown above. It is just a coordinate transformation; the position of point $P_{r\to\varnothing\theta\to r''}$ and its corresponding vector $\boldsymbol{r}_{r\to\varnothing\theta\to r''}$ cannot be changed after the operation. We just try to represent $\boldsymbol{r}_{r\to\varnothing\theta\to r''}$ described in terms of coordinate system $\mathrm{x}''-\mathrm{y}''-\mathrm{z}''$ back to represent $\boldsymbol{r}_{r\to\varnothing\theta\to r''}$ in terms of coordinate system $\mathrm{x}-\mathrm{y}-\mathrm{z}$. From examining the three coordinate systems $\mathrm{x}''-\mathrm{y}''-\mathrm{z}''$, $\mathrm{x}'-\mathrm{y}'-\mathrm{z}'$, and $x-y-z$, we can get the coordinate connection relationship among the three coordinate systems.

$$\left\{\begin{array}{c} \widehat{x''} = \cos\theta\widehat{x'} + \sin\theta\left(-\widehat{z'}\right) = \left(\cos\theta\cos\varnothing\hat{x} + \cos\theta\sin\varnothing\hat{y}\right) + \left(-\sin\theta\hat{z}\right) \\ \widehat{y''} = \widehat{y'} = -\sin\varnothing\hat{x} + \cos\varnothing\hat{y} \\ \widehat{z''} = \sin\theta\widehat{x'} + \cos\theta\widehat{z'} = \left(\sin\theta\cos\varnothing\hat{x} + \sin\theta\sin\varnothing\hat{y}\right) + \left(\cos\theta\hat{z}\right) \end{array}\right\} \quad (6)$$

So then we can write down the transformation matrix between coordinate systems $x-y-z$ and $\mathrm{x}''-\mathrm{y}''-\mathrm{z}''$. The transformation matrix transforms the vector rp $\boldsymbol{r}_{p_{r\to\varnothing\theta\to r''}}$ represented in terms of coordinate system $\mathrm{x}''-\mathrm{y}''-\mathrm{z}''$ back to $\boldsymbol{r}_{p\varnothing\theta}$ represented in terms of coordinate system $\mathrm{x}-\mathrm{y}-\mathrm{z}$,

$$\begin{pmatrix} x_{p\varnothing\theta} \\ y_{p\varnothing\theta} \\ z_{p\varnothing\theta} \end{pmatrix}_{r} = \begin{pmatrix} \cos\theta\cos\varnothing & -\sin\varnothing & \sin\theta\cos\varnothing \\ \cos\theta\sin\varnothing & \cos\varnothing & \sin\theta\sin\varnothing \\ -\sin\theta & 0 & \cos\theta \end{pmatrix} \begin{pmatrix} x' \\ y' \\ z' \end{pmatrix}_{r'} \quad (7)$$

Contracted form about this transformation is

$$\boldsymbol{r}_{p_{\varnothing\theta}} = U_{\boldsymbol{r'}\to\boldsymbol{r}}\boldsymbol{r}_{p_{r\to\varnothing\theta\to r'}} \quad (8)$$

with transformation matrix

$$U_{\boldsymbol{r'}\to\boldsymbol{r}} = \begin{pmatrix} \cos\theta\cos\varnothing & -\sin\varnothing & \sin\theta\cos\varnothing \\ \cos\theta\sin\varnothing & \cos\varnothing & \sin\theta\sin\varnothing \\ -\sin\theta & 0 & \cos\theta \end{pmatrix} \quad (9)$$

Finally, we can obtain the transformation matrix $U_{\varnothing\theta}$ which transforms the original given point p; represented by the vector $\boldsymbol{r}_p$ in terms of coordinate system $x-y-z$, into a new point $p_{\varnothing\theta}$, represent by the vector $\boldsymbol{r}_{p\varnothing\theta}$ in terms of coordinate system $x-y-z$, when the oblique operation has performed.

$$U_{\varnothing\theta} = \boldsymbol{U}_{\boldsymbol{r'}\to\boldsymbol{r}}\boldsymbol{U}_{r\to\varnothing\theta\to r'} \quad (10)$$

The explicit form of $U_{\varnothing\theta}$ is

$$U_{\varnothing\theta} = \begin{pmatrix} \sin^2\varnothing + \cos^2\varnothing\cos\theta & -\cos\varnothing\sin\varnothing + \sin\varnothing\cos\varnothing\cos\theta & \sin\theta\cos\varnothing \\ -\sin\varnothing\cos\theta + \cos\varnothing\cos\theta\sin\varnothing & \cos^2\varnothing + \sin^2\varnothing\cos\theta & \sin\theta\cos\varnothing \\ -\cos\varnothing\sin\theta & -\sin\varnothing\sin\theta & \cos\theta \end{pmatrix} \quad (11)$$

Here, we find that the operation shown in Eq. 3 is retrieved by operated under the asymmetric rolling principle transformation

$$\boldsymbol{r}_{p_{\varnothing\theta}} = \boldsymbol{U}_{\boldsymbol{r'}\to\boldsymbol{r}}\boldsymbol{r}_{p_{r\to\varnothing\theta\to r'}} = \boldsymbol{U}_{\boldsymbol{r'}\to\boldsymbol{r}}\boldsymbol{U}_{r\to\varnothing\theta\to r'}\boldsymbol{r}_p = U_{\varnothing\theta}\boldsymbol{r}_p \quad (12)$$

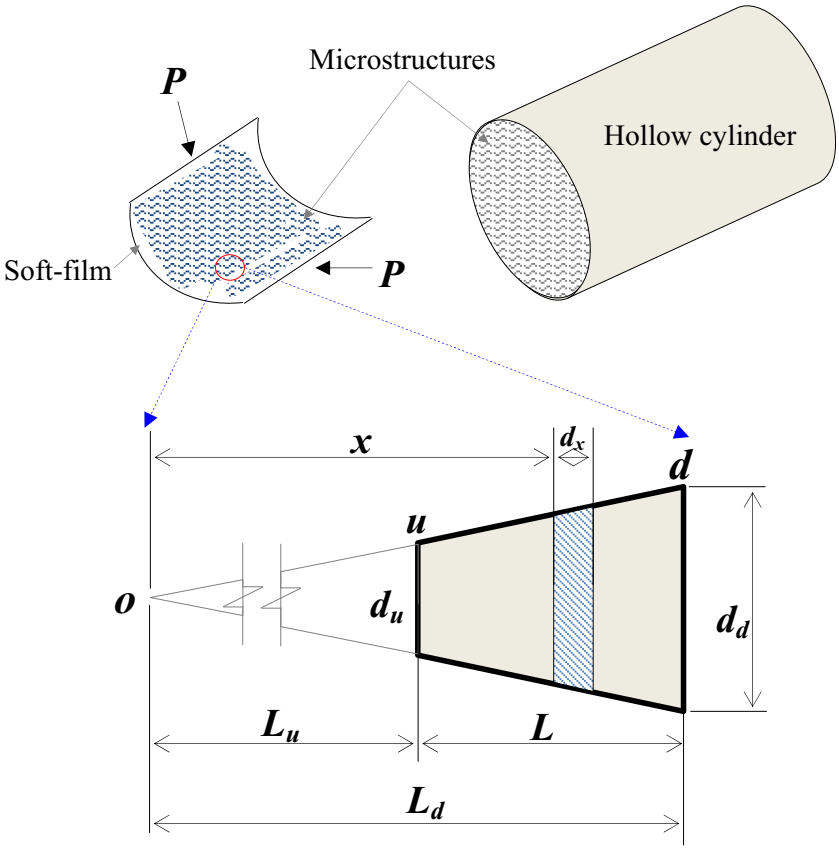

Fig. 3 Schematic diagram of the microdeformation of the feature size of the cone-shaped microstructure

2.3 Calculation method of the microstructure curved surface's microdeformation

The preparation of the roller mold core is a part of the deformation. This section discusses the cone-shaped structure. During the preparation of the roller microstructure mold core, the master pattern of the microstructure (attached with large-area film) must be attached to the inner layer of the designed hollow cylinder. When attached, the microstructure is subject to bending extrusion force, and the side force is relatively larger than the vertical force. It is assumed that, during the attachment and bending process, the force applied on microstructure (axial force) P may change the boundary dimension of the microstructure. Figure 3 shows the schematic diagram of the microdeformation of the feature size of the cone-shaped microstructure.

$$L_u/L_d = d_u/d_d = x/d(x)$$
$$d(x) = d_u x/L_u$$
$$u(x) = \pi(d(x))^2/4 = \pi d_u^2 x^2/4{L_u}^2$$

Therefore, the vertical microdeformation can be expressed as

$$\delta = \int_{L_u}^{L_d}(N(x)dx/Eu(x)) = \int_{L_u}^{L_d}\left(Pdx\left(4L_u^2\right)/E\left(\pi d_u^2 x^2\right)\right)$$
$$= \left(P\left(4L_u^2\right)/E\pi d_u^2\right)\int_{L_u}^{L_d}\left(dx/x^2\right)$$
$$= \left(4PL_u^2/E\pi d_u^2\right)\left[(-1/x)\right]_{L_u}^{L_d}$$
$$= \left(4PL_u^2/E\pi d_u^2\right)\left((1/L_u)-(1/L_d)\right)$$

After the integral, vertical microdeformation amount is, as shown as (Eq. 13),

$$\delta = 4PL/\pi E d_u d_d \tag{13}$$

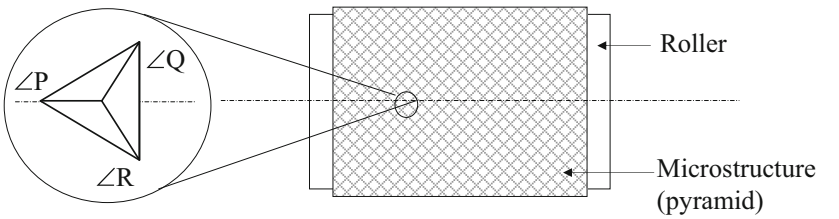

Fig. 4 Characteristic dimensions of the original microstructure pattern on the roller

where δ is vertical microdeformation of the microstructure, L is the height of the microstructure, d_u is the top diameter of the microstructure, d_d is the bottom diameter of the microstructure, and P is the force applied on the microstructure during the bending process.

The vertical microdeformation obtained by the calculation is considered for the minor correction of the feature size of the microstructure in this study.

2.4 Microstructure asymmetric forming simulation and angle assessment prediction method

This study adopted the asymmetric force application method and predicted that the microstructure would have asymmetric performance after roller inclination angle ($\angle\alpha$) was formed through R2P. Matlab software simulation was used for assessment and verification. The complex pyramid microstructure was used as the research spindle. The relationship between the formability and the asymmetric inclination angle of the roller after R2P was discussed. Figure 4 shows the characteristic dimensions of the original microstructure pattern on the roller, where the bisector of its one corner ($\angle$P) is parallel to the axis of the roller. As the pyramid microstructure is symmetrical to the axis of the parallel roller, the angle of the original roller microstructure is $\angle P=\angle Q=\angle R = 60°$. The calculation shows that the corner $\angle$P, $\angle$Q or $\angle$P, $\angle$R of the microstructure, which is R2P to the UV resist, can be measured, and the asymmetric roller inclination angle ($\angle\alpha$) can be obtained with the inverse method, in order to verify the accuracy of the asymmetric R2P after the roller inclination angle.

The implementation method of this part applies equal gas force (δ) to both ends of the roller, which causes the spring force support of (F_s) to have different spring deformation and position (δ), as shown in Eq. 14.

$$F_s = K \cdot \delta \tag{14}$$

After embossing evenly for a certain depth, the inclined angle force is applied on one side to provide the inclination angle of the roller, that is the initial depression angle ($\angle\alpha$) of the asymmetric R2P defined in this study. The actual R2P results were used to compare with the simulation results on the roller inclination angle as predicted by Matlab software. The findings can be used for the assessment of the actual R2P and simulation accuracy.

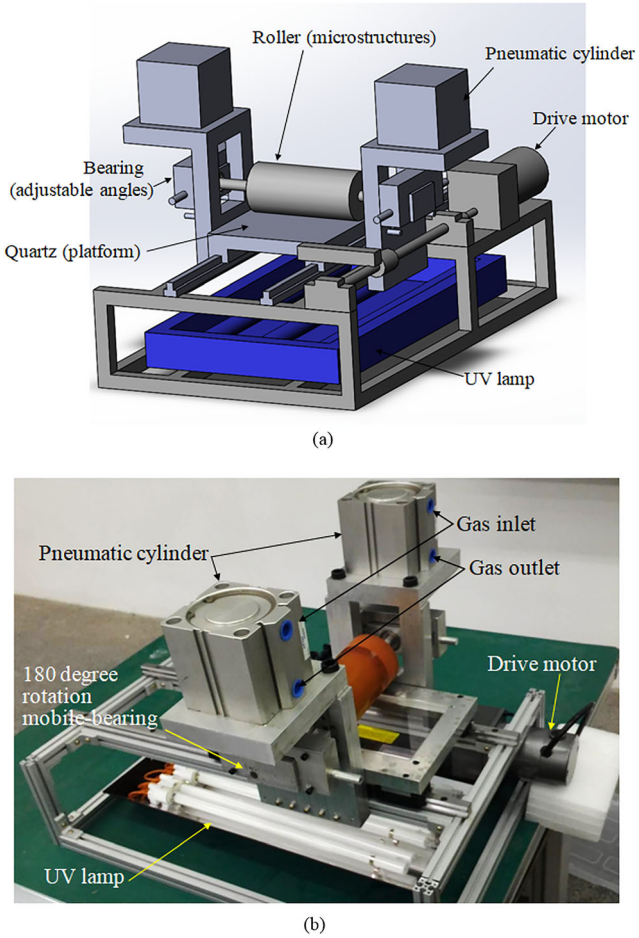

Fig. 5 Asymmetric R2P system's machine system. **a** Schematic diagram. **b** Actual diagram

3 Experimental

3.1 Design and production of the machine of the asymmetric R2P system

The asymmetric R2P system researched and developed in this study includes three main action parts: the drive part of the

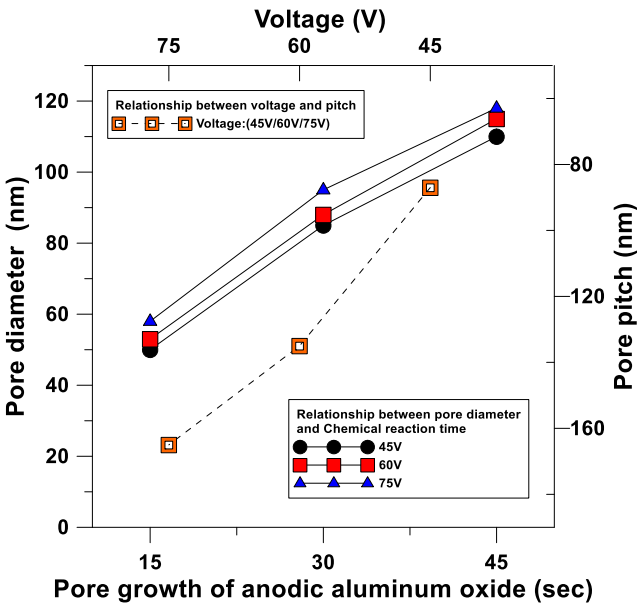

Fig. 6 Obtain the required aluminum nanostructure holes through adjusting the temperature, voltage (45, 60, and 75 V), and pore-enlargement time

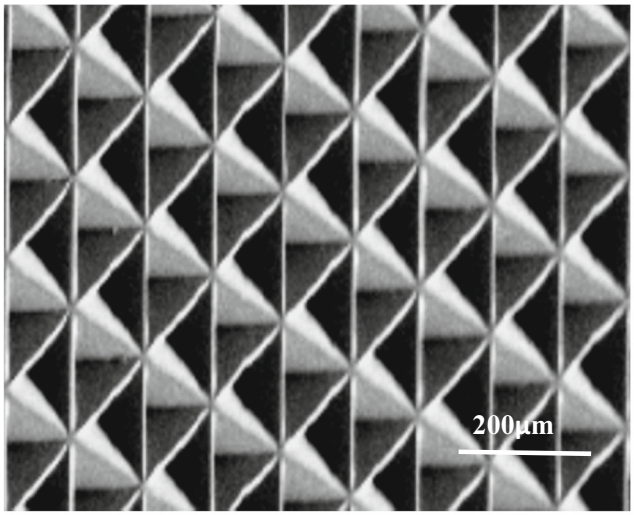

(a)

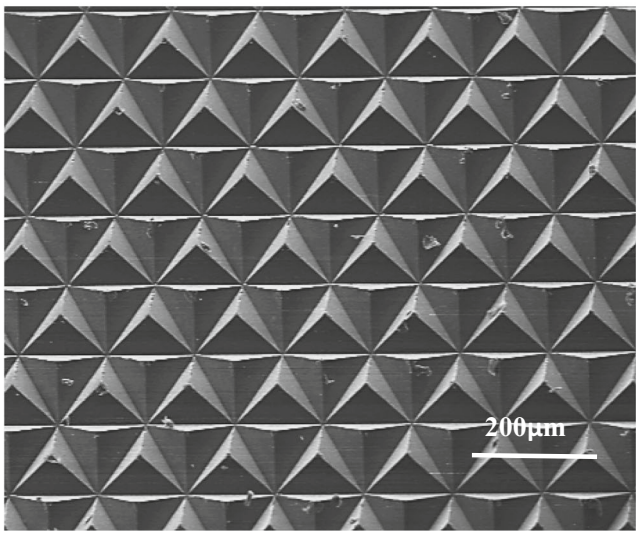

(b)

Fig. 7 Use the MENS process to produce pyramid microstructures. **a** Pyramid (equilateral triangle cone) microstructure. **b** Gas-assisted slight hot-pressing technology to duplicate the complementary-shaped microstructure

(a)

(b)

Fig. 9 Use pressure-sensitive film to test the R2P uniformity of the R2P system applied with **a** symmetric and **b** asymmetric force

ultraviolet-light diode (UV-LED) and embossing platform, the R2P part of the microstructure roller, and the asymmetric angle control part, as shown in Fig. 5. During the R2P process, the control roller generates the inclination angle through the application of different gas forces. In order that the inclination angle of the bearing is fully represented, this study innovatively designed the 180° rotation mobile bearing on both ends of the roller, which is the main method for controlling the asymmetric embossing angle.

3.2 Methods of microstructure mold preparation, seamless roller preparation, and UV resist

3.2.1 Application of anodic oxidation technology to produce nanohole mold

Molds were prepared using conventional anodic oxidation techniques. In this study, preprocessed 99.999% pure

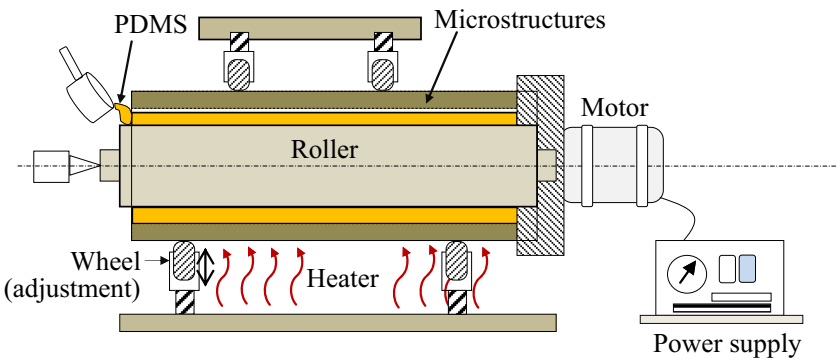

Fig. 8 Production system of impending shaft-type seamless roller

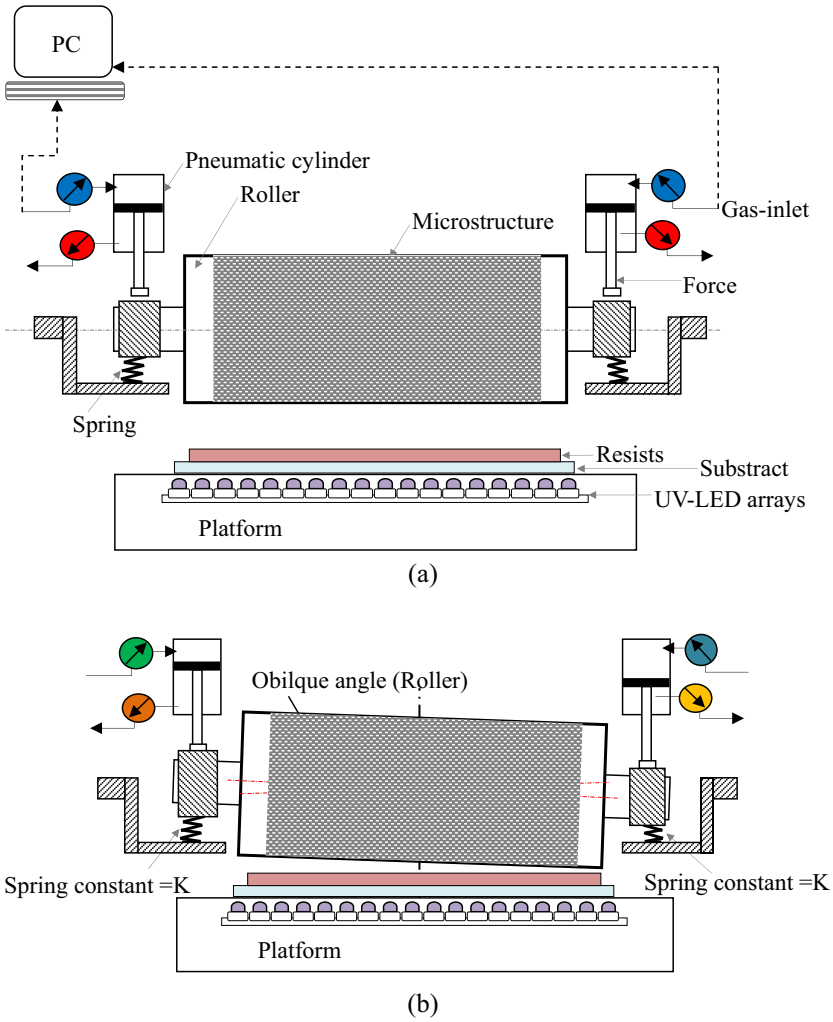

Fig. 10 R2P test process

aluminum was used to obtain the required aluminum nanostructure holes (Fig. 6), which was achieved by taking the oxalic acid as the electrolyte and adjusting the temperature, voltage (45, 60, and 75 V), and pore-enlargement time.

3.2.2 Application of the MENS process to produce a pyramid array microstructure

The third original mold used the MENS process (it is not detailed here as it is a commonly used technology) to produce the pyramid array microstructure with the side length of 165 μm. The prepared microstructure used the gas-assisted slight-hot-pressing technology to conduct the embossing and replication of the complementary PC material microstructure, as shown in Fig. 7. The prepared microstructure was then attached completely to inner spindle's hole wall in sequence. The driving wheel, along with adjusting the microstructure inclination angle of inner spindle's hole wall, was used to ensure the complete filling of the roller. The coherent power supply was used to control the rotating speed of the roller during the seamless filling process. The solution of PDMS (poly-dimethylsiloxan, Sylgard ™ 184, Dow Corning), which was diluted with toluene, was diffused into the nanostructure to conduct more complete filling flow (this step can be omitted for the micron-structure). Heat was applied to accelerate curing, in order to produce the innovative impending shaft-type seamless roller of this study, as shown in Fig. 8. This study used PDMS with high hydrophobicity and excellent material properties (abrasion resistance and fatigue resistance) as the microstructure mold material for embossing. After preparation, three kinds of microstructures were obtained, including the microlens array, (nano/microhole), pyramid array, which covers the PDMS microstructure mold on the outer layer of the roller. The resist used UV-curing resin (SU8 and Acu-Coat UV3215B) as the material for R2P replication.

3.3 R2P uniformity test method of the roller and mechanical properties test of the soft mold material

The pressure-sensitive film was used as the test method for initial R2P uniformity and asymmetry. Under the pressure within the range of specification, the pressure-sensitive film

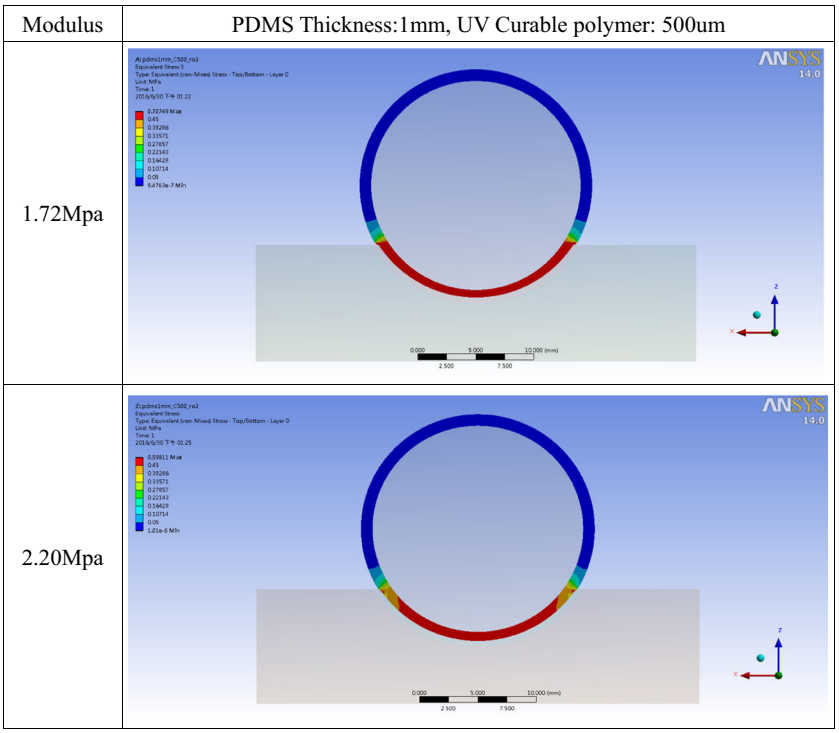

Fig. 11 Simulation of pressure distribution on the microstructure mold thickness under the conditions of applying 0.1-MPa force with 1-mm mold thickness and different elastic modulus of 1.72 and 2.20 MPa

used in this study had the function of a color-developing agent and cracked particulate chromosphere. Different pressures resulted in a display of different color depths. This study used the soft model without a microstructure to conduct R2P testing, and the results showed the system's uniformity of the symmetrical R2P and grayscale pressure color performance of asymmetric force, as shown in Fig. 9.

3.4 Asymmetric grayscale R2P forming steps

This study used the self-designed and developed asymmetric R2P machine to conduct the R2P forming process. The experimental procedure is as follows: (a) spinning coating UV curing resist on the substrate (polycarbonate (PC) or polymethyl methacrylate (PMMA)) with

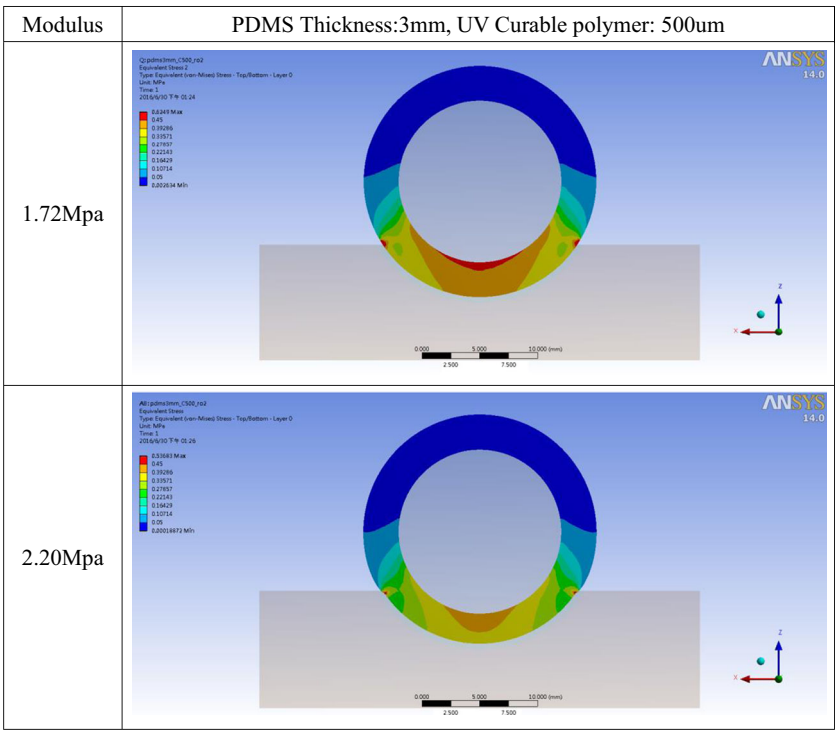

Fig. 12 Simulation of pressure distribution on the microstructure mold thickness under the conditions of applying 0.1-MPa force with 3-mm mold thickness and different elastic modulus of 1.72 and 2.20 MPa

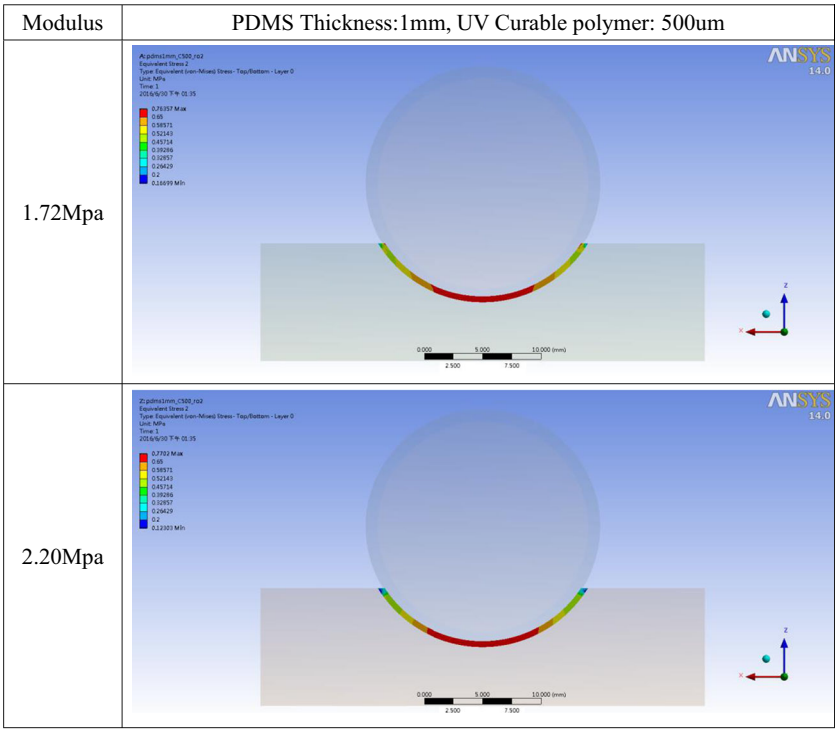

Fig. 13 Simulation of pressure distribution on the UV resist under the conditions of applying 0.1-MPa force with 1-mm mold thickness and different elastic modulus of 1.72 and 2.20 MPa

the roll coating method, then place it on the quartz glass mobile platform of the R2P system; (b) use the asymmetric (or symmetrical) force application method, set the embossing force, determine the roller inclination angle ($\angle\alpha$), adjust the R2P parameters, turn on the UV light for simultaneous curing to conduct R2P exposure cure forming, and obtain the finished product, as shown in Fig. 10.

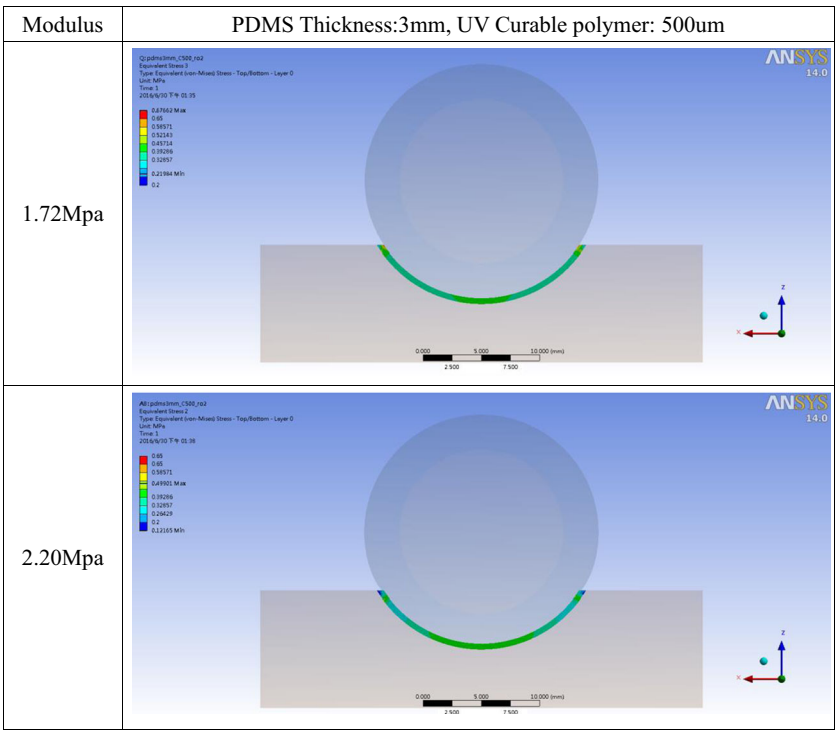

Fig. 14 Simulation of pressure distribution on the UV resist under the conditions of applying 0.1-MPa force with 3-mm mold thickness and different elastic modulus of 1.72 and 2.20 MPa

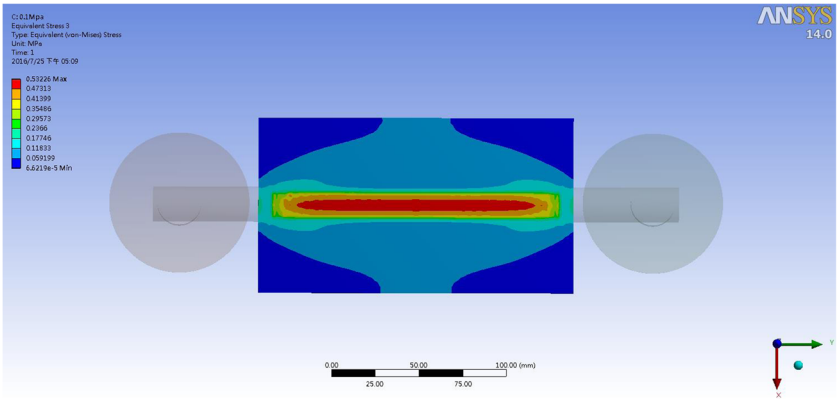

(a)

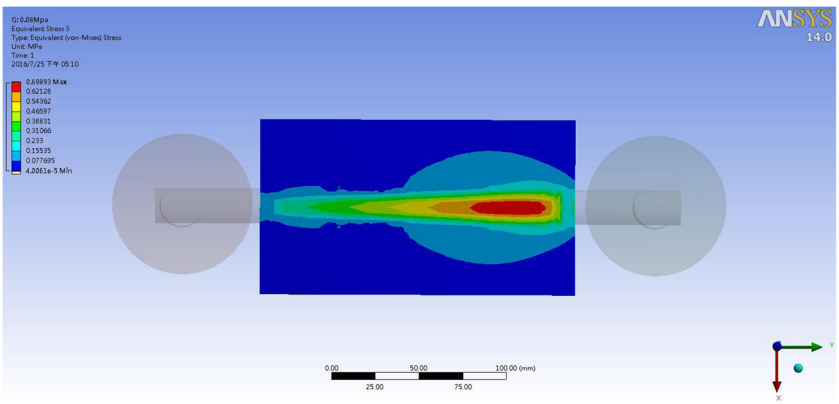

(b)

Fig. 15 Simulation analysis of the force on the substrate plate under the conditions **a** applied with symmetric force (left, 0.1 MPa; right, 0.1 MPa) and **b** applied with asymmetric force (left, 0.08 MPa; right, 0.1 MPa)

4 Results and discussion

4.1 Analysis of the influence of the system force condition under the simulated asymmetric grayscale force

4.1.1 Influence of roller mold thickness and material mechanical properties on the R2P contact pressure distribution

In order to fully show the pressure distribution of the roller mold thickness and elastic modulus, this study conducted direct pressure simulation by designing a concave surface and roller of nearly a 1/4 circle arc. Cross-comparison of the analysis results showed that, under the same force of 0.1 MPa, respective simulations under the conditions of different PDMS mold thicknesses of 1 and 3 mm, as well as different elastic modulus of 1.72 and 2.20 MPa, the lower elastic modulus of the material and the microstructure mold were subject to higher pressure with large distribution and wide range. As for a thicker mold, its contact with aluminum will show higher pressure distribution, higher stress distribution, and wider distribution on its contact with the R2P material, as shown in Figs. 11 and 12. In terms of the R2P material (with the UV resist of 500-μm thickness), when the microstructure layer had thick mold, the elastic modulus provided higher and wider pressure distribution to the resist, as shown in Figs. 13 and 14.

4.1.2 Influence on roller contact pressure distribution under the condition of different forces on both ends of the roller

Asymmetric R2P simulation was carried out by simulation software. The force condition and related influence of the roller and the substrate plate under asymmetric force were discussed. This study simulated the pressure distribution under the condition of equal force and unequal force on both ends of the roller. The results showed that, regarding the force condition of the substrate plate when applying equal forces of 0.1 and 0.1 MPa, as well as applying unequal forces of 0.1 and 0.08 MPa (Fig. 15), the symmetrical force was uniform. Moreover, there was significant grayscale pressure distribution under asymmetric force.

4.2 Discussion of anodic oxidation process micro/nanoscale structure mold core and asymmetric R2P

The micro/nanoscale structure was obtained by the anodic oxidation process, through gas-assisted hot-pressing, and it was

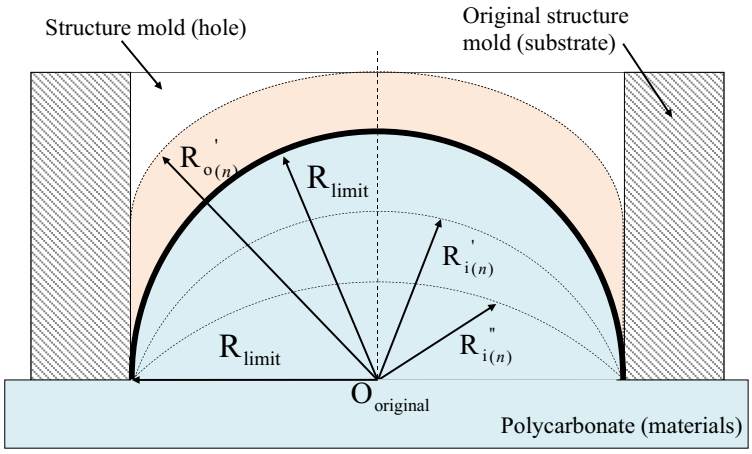

(a)

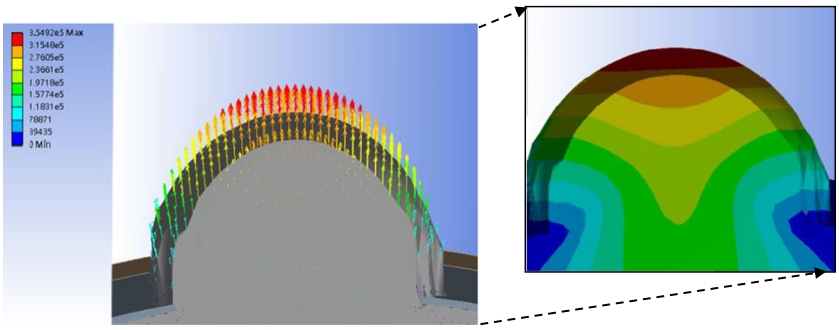

(b)

Fig. 16 **a** Schematic diagram of the radius limit of the formed micro/nanoscale spherical lens. **b** Stress distribution and vector distribution of the simulated forming spherical lens' radius (R_{limit})

convex micro/nanoscale structure. Figure 16a shows the radius limit (R_{limit}) of the micro/nanoscale spherical lens of the replica molding with the thick solid line. The spherical or aspheric

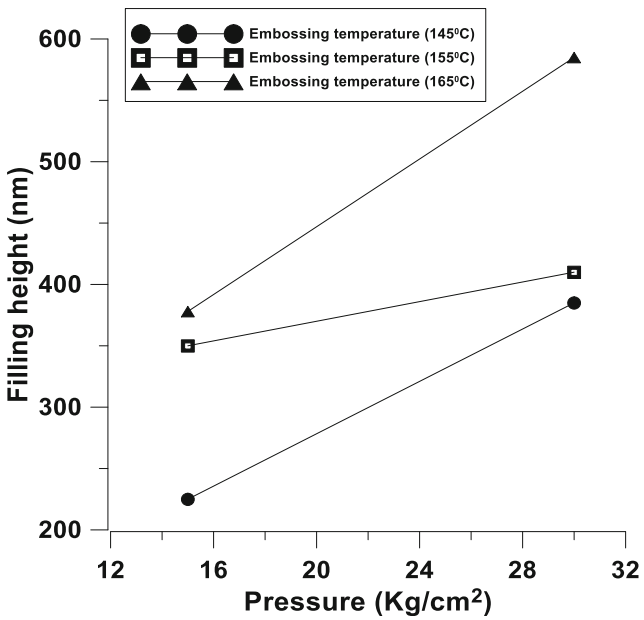

Fig. 17 Influence of the formability of gas-assisted hot-pressing anodic oxidation hole mold under different experimental conditions

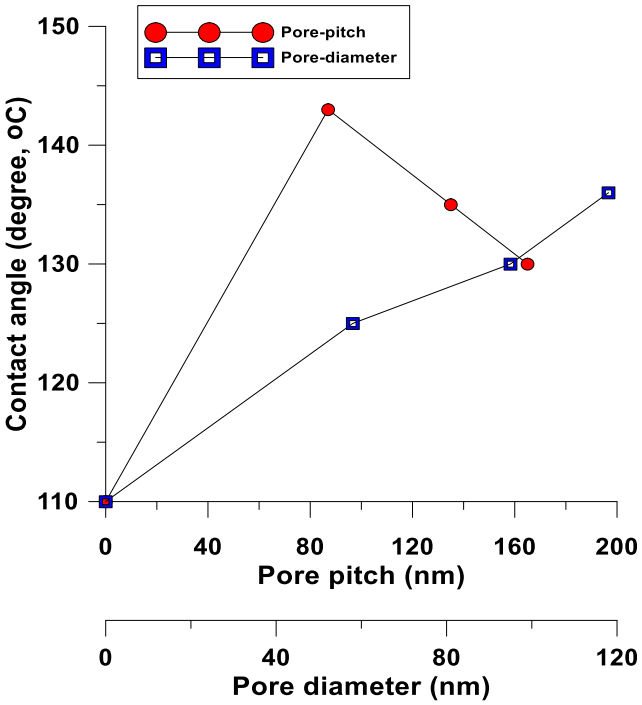

Fig. 18 Influence of micro/nanoscale scale structure with different sizes on the contact angle

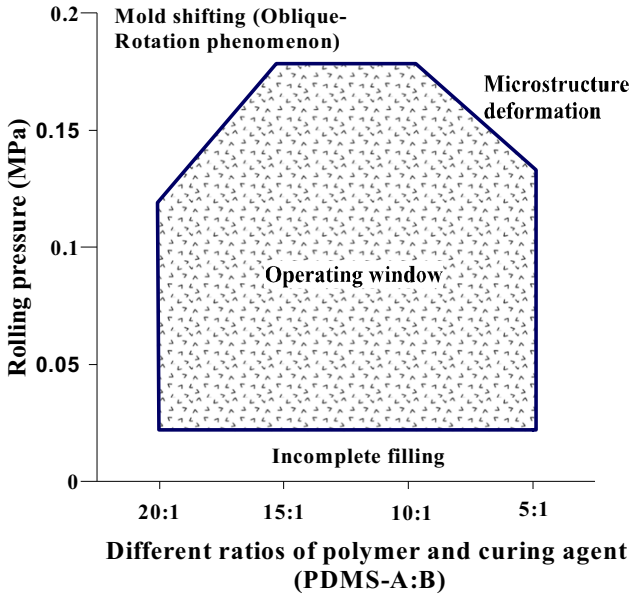

Fig. 19 Range of partial microstructure's slight inclined-rotation phenomenon and forming operation window in the R2P forming area

surfaces less than ($R'_{i(n)}$, $R''_{i(n)}$) or greater than ($R'_{o(n)}$) the spherical lens radius limit are shown by a dotted line. Figure 16b simulates the stress distribution of the radius limit that forms the spherical lens, which uses the impending shaft-type seamless roller to produce the micro/nanoscale structure roller and the asymmetric grayscale R2P test. The results showed the influence of the anodic oxidation process and gas-assisted hot-pressing conditions (temperature and pressure). This study used a micro/nanoscale mold with 75 V and pore pitch = 165 nm for discussion and found that the formability of the PC substrate was improved as the temperature and pressure of the hot-pressing replication increased, as shown in Fig. 17. The impending shaft-type seamless roller was used to produce the roller mold core (concave). Asymmetric R2P can achieve a micro/nanoscale scale structure with unequal grayscale size. The experiment of the liquid drop contact angle proved that different sizes of micro/nanoscale scale structures affect hydrophobicity. The higher density and smaller scale of the microstructure would lead to greater contact angle (high hydrophobicity), as shown in Fig. 18.

4.3 Discussion of the accuracy of the asymmetric grayscale R2P simulation of the microstructure and its correction

Figure 19 shows the forming operating range of the proposed system. Under the condition that the flexible microstructure mold core is too soft, it shows that the opportunity for the slight inclined-rotation effect of the microstructure occurs between the R2P. This experiment found that the ratio of the soft mold's AB agent (resist and curing agent) was low (A/B, 15:1). When the strength of the soft mold was low, there was slight inclined-rotation phenomenon (O-R phenomenon) during the R2P process. In addition, various factors, such as dispersion uniformity and the mechanical properties of the microstructure, affected the accuracy of the R2P. Therefore, this study chose to add the rotation angle ($\angle\beta$), as well as the change between $-2°$ to $2°$. At the same time, the original roller inclination angle ($\angle\alpha$) was set asymmetrically from $-5°$ to $5°$. The simulation results showed that, without considering the inclined-rotation effect, the measurement angle ($\angle$P) of the symmetrical end angle had approximate linear performance after R2P, in comparison with the simulated roller inclination angle ($\angle\alpha$), as shown in Fig. 20. Considering the case of slight inclined-rotation effect ($\angle\beta$) and roller inclination angle ($\angle\alpha$) shows the curved surface-like distribution performance after simulation was symmetrical with the inclined-rotation angle of 0 degrees, as shown in Fig. 21.

4.4 Discussion of the actual R2P angle and simulated prediction assessment of the asymmetric grayscale R2P forming of the microstructure

By introducing the symmetrical end corner ($\angle$P) of asymmetric R2P forming into the simulated correspondence of this

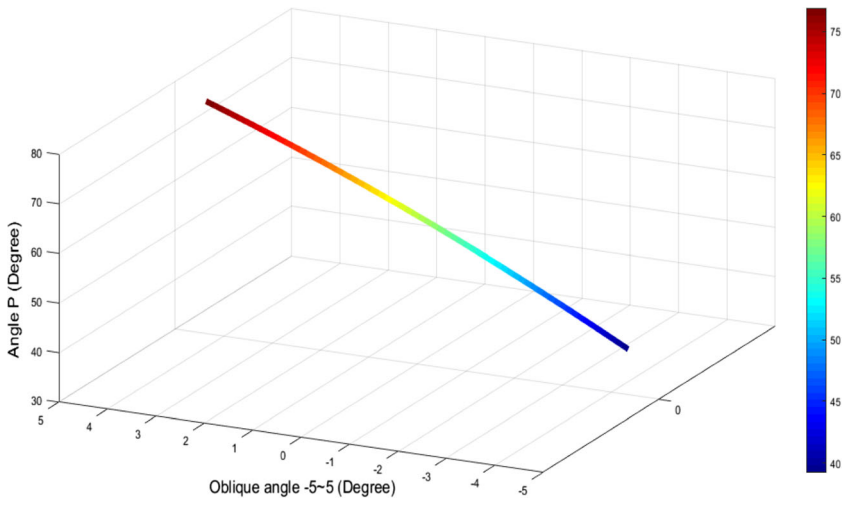

Fig. 20 Relative changes of the measurement angle of the symmetrical end angle ($\angle$P) and the roller inclination angle ($\angle\alpha$)

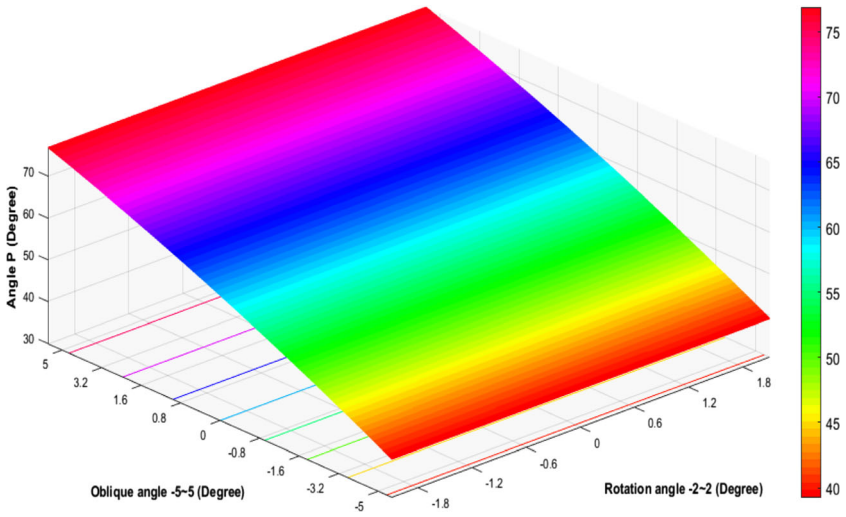

Fig. 21 Measurement angle of the symmetrical end angle (∠P) under the condition of considering the slight inclined-rotation effect (∠β) and the roller inclination angle (∠α)

study, the original roller inclination angle (∠α) could be obtained. After several unequal asymmetric force forming tests, the corresponding R2P inclination angle accuracy was obtained. Regarding the partial microstructures that obtain inclined-rotation angle (∠β) forming due to the material, they could stably obtain the roller inclination angle. Based on the inclined-rotation angle, as obtained by the relationship between different R2P depths and the corresponding material surface areas, the roller inclination angle could be obtained using the inverse method. The variation trend of the surface

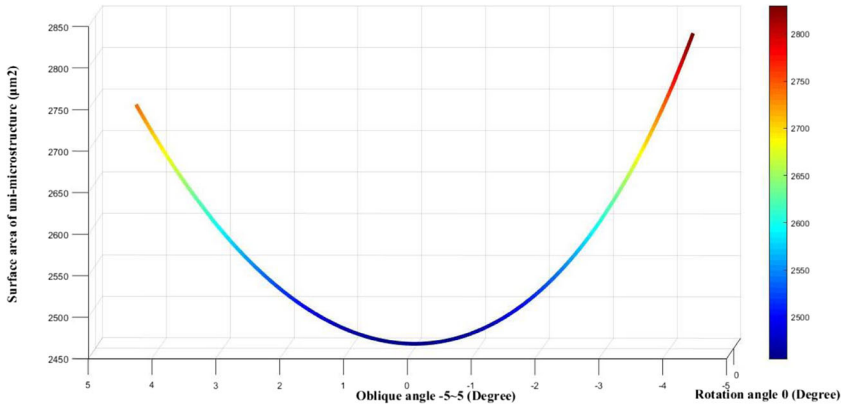

(a)

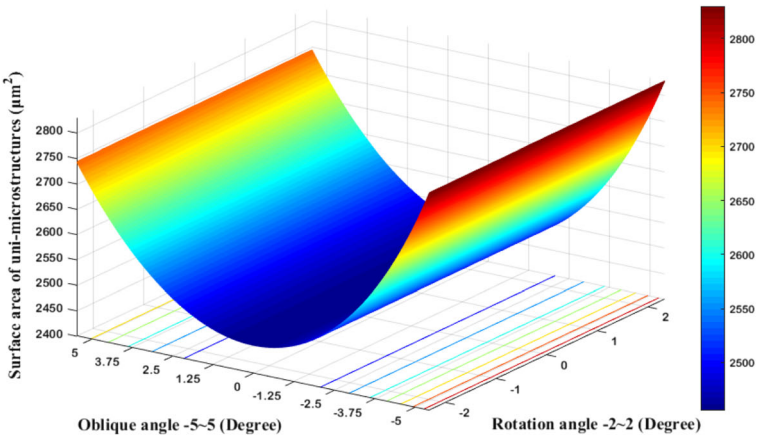

(b)

Fig. 22 Variation trend of the surface area with 10-μm R2P depth after asymmetric r2p forming under the condition of **a** only considering the roller inclination angle (∠α) and **b** considering the slight inclined-rotation effect (∠β) and the roller inclination angle (∠α)

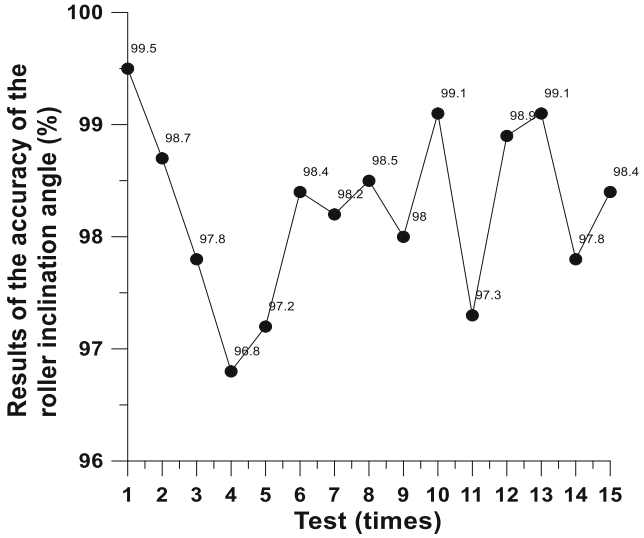

Fig. 23 Results of the accuracy of the roller inclination angle corresponding to the unequal asymmetric force

area at different locations, after asymmetric R2P forming (Fig. 22), brings it into the simulated prediction angle. The roller inclination angle ($\angle\alpha$) can be determined. The analysis results showed that, after several unequal asymmetric force forming tests, the corresponding R2P inclination angle accuracy could be obtained, as shown in Fig. 23.

5 Conclusions

This study developed the asymmetric grayscale R2P processing technology. It first designed and set up the system, and then simulated the force condition of the asymmetric force on the roller, in order to make synchronous corrections on the design sketch of the system equipment. This study conducted simulation and prediction on the R2P angle of the asymmetric microstructure, as well as the assessment of the arrangement, and carries out actual R2P test was conducted. The results showed that the proposed system could produce the grayscale microstructure by R2P. Through the feature size of the actual R2P result, the simulation assessment method could obtain accurate roller inclination angles of the actual roller under asymmetric force with the inverse method. Therefore, it is possible to provide assessment before R2P for the actual production end in the future. The proposed novel technology was proven to be an effective assessment for microstructure R2P replication based on .

Acknowledgments This work was partially supported by the Ministry of Science and Technology (Series No. MOST 105-2221-E-415-005) of Taiwan, Republic of China.

References

1. Huang P, Kang J, Zhao Y, Chen S, Han R, Zhou Z, … & Liu X (2016) Reconfigurable nonvolatile logic operations in resistance switching crossbar array for large-scale circuits. Adv Mater 28(44), 9758–9764
2. Santos TG, Miranda RM, de Carvalho CC (2014) A new NDT technique based on bacterial cells to detect micro surface defects. NDT&E INT 63:43–49
3. Chang WH, Wang CH, Lin CL, Wu JJ, Lee MS, Lee GB (2015) Rapid detection and typing of live bacteria from human joint fluid samples by utilizing an integrated microfluidic system. Biosens Bioelectron 66:148–154
4. Fang YC, Cheng DL, Huang JW (2015) Optical design of external illuminance for display backlight module. J Disp Technol 11(12): 979–986
5. Fang YC, Tzeng YF, Wu KY (2014) A study of integrated optical design and optimization for LED backlight module with prism patterns. J Disp Technol 10(10):812–818
6. Chen RH, Weng YJ, Yang SY (2016) Magnetic fluid microstructure curved surface uniform embossing and photocuring process technology. Polym Adv Technol 5:630–641
7. Weng YJ, Tsai J (2016) Application of 9× 9 grid gas bags pressure control technology to imprinting of various microstructures. OPTIK 127(20):8638–8645
8. Fiorillo M, Verre AF, Iliut M, Peiris-Pagés M, Ozsvari B, Gandara R et al (2015) Graphene oxide selectively targets cancer stem cells, across multiple tumor types: implications for non-toxic cancer treatment, via "differentiation-based nano-therapy". Oncotarget 6(6):3553–3562
9. Chen Q, Liang C, Wang X, He J, Li Y, Liu Z (2014) An albumin-based theranostic nano-agent for dual-modal imaging guided photothermal therapy to inhibit lymphatic metastasis of cancer post surgery. Biomaterials 35(34):9355–9362
10. Argyros A (2013) Microstructures in polymer fibres for optical fibres, THz waveguides, and fibre-based metamaterials. ISRN Optics 2013
11. Weng YJ (2015) UV-curable technique of magnetic roller soft mold and microstructure pattern replication. Int Polym Process 30(1):63–69
12. Nie W, Chen F (2015) Dual-line optical waveguides in cu: KNSBN crystal fabricated by direct femtosecond laser writing. Opt Eng 54(9):097106–097106
13. Chen RH, Weng YJ, Hurng HY, Wang YL, Tsai CT (2016) Study of transfer printing using micro-dynamically-regulated microstructural flexible mold. OPTIK 127(7):3590–3596
14. DUAN MY, SHAN X, AI Y (2014) Research and progress of laser atmospheric turbulence simulator. Optical Communication Technology 1:017
15. Nielsen MP, Lafone L, Rakovich A, Sidiropoulos TP, Rahmani M, Maier SA, Oulton RF (2016) Adiabatic nanofocusing in hybrid gap plasmon waveguides on the silicon-on-insulator platform. Nano Lett 16(2):1410–1414
16. Wu D, Niu LG, Wu SZ, Xu J, Midorikawa K, Sugioka K (2015) Ship-in-a-bottle femtosecond laser integration of optofluidic microlens arrays with center-pass units enabling coupling-free parallel cell counting with a 100% success rate. Lab Chip 15(6):1515–1523
17. Yong J, Chen F, Yang Q, Du G, Bian H, Zhang D, … & Hou X (2013) Rapid fabrication of large-area concave microlens arrays on PDMS by a femtosecond laser. ACS Appl Mater Interfaces 5(19): 9382–9385
18. Oliver WC, Pharr GM (1992) An improved technique for determining hardness and elastic modulus using load and displacement sensing indentation experiments. J Mater Res 7(6):1564–1583
19. Oliver WC, Pharr GM (2004) Measurement of hardness and elastic modulus by instrumented indentation: advances in understanding and refinements to methodology. J Mater Res 19(1):3–20